



Article

Stability Analysis of Unsteady MHD Rear Stagnation Point Flow of Hybrid Nanofluid

Nurul Amira Zainal ^{1,2}, Roslinda Nazar ^{1,*}, Kohilavani Naganthran ^{1,3,4} and Ioan Pop ⁵

- ¹ Department of Mathematical Sciences, Faculty of Science and Technology, Universiti Kebangsaan Malaysia (UKM), Bangi 43600, Malaysia; nurulamira@utem.edu.my (N.A.Z.); kohl@ukm.edu.my (K.N.)
- ² Fakulti Teknologi Kejuruteraan Mekanikal dan Pembuatan, Universiti Teknikal Malaysia Melaka, Hang Tuah Jaya, Durian Tunggal 76100, Malaysia
- ³ Institute of Mathematical Sciences, Faculty of Science, Universiti Malaya, Kuala Lumpur 50603, Malaysia
- ⁴ Center for Data Analytics, Consultancy and Services, Faculty of Science, Universiti Malaya, Kuala Lumpur 50603, Malaysia
- ⁵ Department of Mathematics, Babeş-Bolyai University, R-400084 Cluj-Napoca, Romania; popm.ioan@yahoo.co.uk
- * Correspondence: rmn@ukm.edu.my

Abstract: Previous studies have reported that investigating the stagnation point flow is relevant in a variety of industrial and technological processes, including extrusion and the polymer industries. Hence, the present work aims to analyse the heat transfer performance of unsteady magnetohydrodynamics (MHD) in hybrid nanofluid and heat generation/absorption impact. The multivariable differential equations with partial derivatives are converted into a specific type of ordinary differential equations by using valid similarity transformations. The resulting mathematical model is clarified utilising the *bvp4c* function. The results of various control parameters were analysed, and it was discovered that increasing the nanoparticle concentration and magnetic field increases the coefficient of skin friction along the stretching/shrinking surface. The inclusion of the heat generation parameter displays an upward trend in the temperature distribution profile, consequently degrading the heat transfer performance. The findings are confirmed to have more than one solution, and this invariably leads to a stability analysis, which confirms the first solution's feasibility.

Keywords: magnetohydrodynamics; heat generation/absorption; stretching/shrinking surface; stability analysis; hybrid nanofluid



Citation: Zainal, N.A.; Nazar, R.; Naganthran, K.; Pop, I. Stability Analysis of Unsteady MHD Rear Stagnation Point Flow of Hybrid Nanofluid. *Mathematics* **2021**, *9*, 2428. <https://doi.org/10.3390/math9192428>

Academic Editor: Mario Versaci

Received: 26 July 2021

Accepted: 20 September 2021

Published: 30 September 2021

Publisher's Note: MDPI stays neutral with regard to jurisdictional claims in published maps and institutional affiliations.



Copyright: © 2021 by the authors. Licensee MDPI, Basel, Switzerland. This article is an open access article distributed under the terms and conditions of the Creative Commons Attribution (CC BY) license (<https://creativecommons.org/licenses/by/4.0/>).

1. Introduction

In real-world applications, the magnetic field is crucial in altering the field of flow. The analysis of MHD in boundary layer flow is essential in the industry because of its persistent demand in a variety of industrial fields, such as metallurgical procedures and petroleum production [1]. Other than that, the MHD models are also particularly relevant in the investigations of controlled thermonuclear fusion, where the vertical instability of the plasma column inside the machine, such as the Tokamak ASDEX or ITER machines, is still a challenge. Controlling plasma dynamics with the inclusion of MHD effect in tokamaks is one of the most important issues in the theoretical and practical study of controlled thermonuclear fusion, as well as in the global transition to fusion power engineering. However, due to the complexity of construction in tokamak plasma properties, the plasma magnetic control approaches are still underexplored [2]. Because of these circumstances, complex mathematical models and the use of high-performance computing technologies are required. The simulation approach and numerical study in plasma control systems are usually beneficial in saving a lot of expensive experimental time [3]. Mitrishkin et al. [2] conducted an experimental and numerical study on a plasma magnetic cascade multiloop control system. Their findings revealed that a quantitative computation of the plasma shape

scenario is required to obtain the most advantageous magnetic control system operating modes. Meanwhile, De Tommasi [4] proposed several control algorithms based on the dynamic model of the plasma magnetic control in tokamak devices. According to their findings, the availability of reliable plant models is a critical aspect in the design and deployment of plasma magnetic controllers.

Dealing with the study of MHD in boundary layer flow, Hartmann [5] pioneered in establishing the principle of laminar flow of an electrically conductive liquid in a homogeneous magnetic field, which led to major research in MHD over the last few centuries. Leibovich [6] performed an investigation toward the MHD flow at a rear stagnation point to study the use of magnetic fields as a valuable tool in a separation process. Katagiri [1] demonstrated the MHD boundary layer separation by investigating the problem of unsteady rear stagnation point in the presence of an applied magnetic field. Later, Pavlov [7] used a uniform transverse magnetic field to investigate the flow of electrically conducting fluids in a boundary layer. A summary of some research that tests the effect of MHD in the boundary layer flow can be reviewed here [8–11]. The findings in [8,9] show that the magnetic parameter is pronounced to have a significant impact on the heat transfer rate. Meanwhile, [10,11] reported that a decrease in the fluid's velocity is caused by the increment of magnetic field's intensity. Therefore, based on the stated literature, we believe that this study has important implications for understanding the crucial role of MHD in boundary layer flow.

Hiemenz [12] and Homann [13] are credited as the introducers of the classic stagnation point problem in two-dimensional flow. Since then, various investigations were conducted that recognised the important role of the stagnation point flow in several industrial and technological processes such as extrusion activity and the polymer industry [14,15]. Proudman and Johnson [16] and Robins and Howarth [17] developed the boundary layer study at a two-dimensional rear stagnation point, while Howarth [18] established the investigation of boundary layer growth at a three-dimensional rear stagnation point flow. In another study, Turkyimazolgu et al. [19] performed the unsteady MHD rear stagnation point in the permeable and deformable sheet, and it is reported that the inclusion of unsteadiness and magnetic parameter consequently allow a major contribution to the working fluid. Since then, many investigators have conducted several reviews on stagnation point flow subject to the heat transfer efficiency, for instance [20–23]. Khashi'ie et al. [20,21] demonstrate that in the stagnation point flow, hybrid nanofluid has a higher heat transfer rate than conventional nanofluid. Meanwhile, Zainal et al. [22,23] show that the thermal performance is declined when the unsteady parameter is involved in the hybrid nanofluid stagnation point flow. Therefore, the aim of this study is to emphasise the significance of the stagnation point flow in hybrid nanofluids, which may be seen in both natural and industrial phenomena.

Many scholars and practitioners have improved the research of heat transfer analysis involving the unsteady flow due to its essential role in transport phenomena. Due to the different time-based conditions, the unsteady flow behaviour represents an odd pattern instead of the steady flow, which disrupted the fluid motion structure and boundary layer separation, as reported by Smith [24] and White [25]. New design techniques that increase system performance, reliability, and cost reduction are possible with a comprehensive knowledge of the unsteady flow practice in industrial procedures [26]. The numerical study of unsteady flow problems was first initiated by Benson et al. [27], while Sears and Telionis [28] examined the boundary layer separation in unsteady flow. Hayat et al. [29] addressed the unsteady flow of nanofluid with magnetic field and double stratification impact toward an inclined stretching surface. Jahan et al. [30] included the regression and stability analyses of unsteady flow in a nanofluid over a permeable stretching/shrinking sheet. Recently, Zainal et al. [8,31] performed several studies involving the unsteady flow and heat transfer numerically. They reported that the unsteady flow revealed a considerable influence on thermal energy effectiveness and boundary layer separation. Up to the present day, a significant series of researches were carried out concerning the unsteady flow and heat transfer focusing on numerous aspects, including [32–35]. According to the findings of

those studies, the unsteadiness parameter has a substantial impact on the operating fluid. Therefore, as part of the effort to properly understand and evaluate the irregular flows and their applications, active investigations of unsteady boundary layers are required.

Temperature differences between two surfaces or inside separate areas of the same object cause the heat transfer process. The heat transfer phenomenon that is disclosed with heat generation/absorption is vital in geophysical, industrial, and bioengineering processes. In particular, the heat generation impact may alter the thermal profile; subsequently, the deposition rate of the particle in electronic chips, semiconductor wafers and also nuclear reactors [36]. Vajravelu and Hadjinolaou [37] investigated the heat transfer characteristics in the laminar boundary layer of a viscous fluid over a stretching sheet with viscous dissipation and internal heat generation. Alsaedi et al. [38] considered the effect of heat parameter on a stagnation point flow with convection heating at the nanofluid surface. Their findings pointed out that the heat generation parameter, as predicted, causes an increase in fluid temperature, while the heat absorption parameter has the opposite effect. Soomro et al. [39] combined the effect of nonlinear radiation and heat parameter on stagnation point flow toward a moving sheet in a nanofluid. The study discovered that the increasing trend in nanoparticle volume fraction and fluid temperature is proportional to an augmentation of the heat generation/absorption parameter. Latterly, the capability of thermal stability and its performance can be assessed from scientific research for its actual industrial applications, which can be found in the literature, such as [40,41].

A comprehensive examination of the previously discussed literature is only possible to a limited extent. According to the available literature, an investigation of heat transfer and the unsteady MHD rear stagnation point flow in $\text{Al}_2\text{O}_3\text{-Cu}/\text{H}_2\text{O}$ still lacks throughout the scientific literature. As a result of the above main questions, the goal of this research is to establish a computational model by performing a numerical analysis using Tiwari and Das' model [42]. Additionally, Takabi and Salehi [43] and Ghalambaz et al. [44] are acknowledged for the thermophysical properties of the operating fluid. Details and explanations of each particular formulations for the thermophysical properties that were employed in this investigation are available in Babu et al. [45] and Hussain et al. [46]. Additionally, the current study used the `bvp4c` approach in the MATLAB software to elucidate the expressed problem. The stability analysis was carried out since the above approach method effectively established more than one solution. The comparison results for certain cases clearly demonstrate good agreement with the available data.

2. Mathematical Modeling

The unsteady MHD rear stagnation-point flow and heat transfer of $\text{Al}_2\text{O}_3\text{-Cu}/\text{H}_2\text{O}$ hybrid nanofluid past a permeable surface are considered, as demonstrated in Figure 1. The impact of heat generation/absorption is also included. It is assumed that the free-stream velocity is given by $u_\infty = -u_0x/(1 - \beta t)$, where u_0 and β are the real number and constant, respectively. Additionally, the wall has a moving velocity along the x -axis with $u_w = u_0x/(1 - \beta t)$, and the wall transpiration velocity in the y -axis is given by $v_w(x, t)$. Further, the wall temperature is given by $T_w(x, t) = T_\infty + T_0x/L(1 - \beta t)$, while the ambient temperature is considered constant which denoted by T_∞ . The size of the nanoparticles is regarded to be uniform. The governing equations of the hybrid nanofluid for continuity, momentum, energy, and concentration by employing the usual boundary layer approximations are written as (Devi and Devi [47]; Zainal et al. [48])

$$\frac{\partial u}{\partial x} + \frac{\partial v}{\partial y} = 0, \quad (1)$$

$$\frac{\partial u}{\partial t} + u \frac{\partial u}{\partial x} + v \frac{\partial u}{\partial y} = \frac{\partial u_\infty}{\partial t} + u_\infty \frac{\partial u_\infty}{\partial x} + \frac{\mu_{hnf}}{\rho_{hnf}} \frac{\partial^2 u}{\partial y^2} - \frac{\sigma_{hnf}}{\rho_{hnf}} B_0^2 (u - u_\infty), \quad (2)$$

$$\frac{\partial T}{\partial t} + u \frac{\partial T}{\partial x} + v \frac{\partial T}{\partial y} = \frac{k_{hnf}}{(\rho C_p)_{hnf}} \frac{\partial^2 T}{\partial y^2} + \frac{Q_s(T - T_\infty)}{(\rho C_p)_{hnf}}, \quad (3)$$

and the boundary conditions are

$$\begin{aligned} v = v_w(x, t), u = \lambda u_w(x, t), T = T_w(x, t), \text{ at } y = 0, \\ u \rightarrow u_\infty(x, t), T \rightarrow T_\infty \text{ as } y \rightarrow \infty. \end{aligned} \tag{4}$$

The velocity component along the x - and y - directions are denoted by u and v , respectively, $v_w(x, t)$ is the wall mass transfer velocity with $v_w(x, t) < 0$ for suction and $v_w(x, t) > 0$ for injection, T is the temperature of the hybrid nanofluid, μ_{hnf} is the dynamic viscosity, ρ_{hnf} is the density, σ_{hnf} is the electrical conductivity, and B_0 is the transverse magnetic field. Further, k_{hnf} is the hybrid nanofluid thermal conductivity, $(\rho C_p)_{hnf}$ is the heat capacity of the hybrid nanofluid and the coefficient of heat generation/absorption is represented by Q_s . The parameter of stretching/shrinking is symbolised by λ with $\lambda > 0$ and $\lambda < 0$ represent the stretching and shrinking surfaces, respectively, while $\lambda = 0$ indicated a static surface. The fluid systems' thermophysical properties are portrayed in Table 1 (see Abu Nada and Oztop [49]) while the correlation coefficient for the hybrid nanofluid is depicted in Table 2 (see Takabi and Salehi [43]; Ghalambaz et al. [44]).

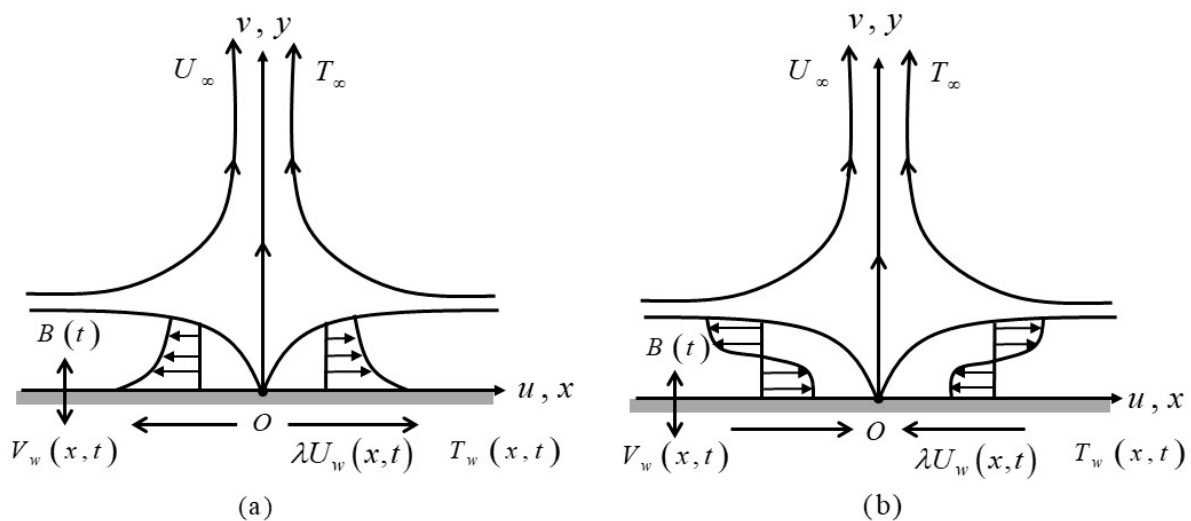


Figure 1. Physical models and coordinate systems: (a) stretching sheet (b) shrinking sheet.

Table 1. The H₂O, Al₂O₃ and Cu thermophysical properties (see Abu Nada and Oztop [49]).

Physical Properties	k (W/mK)	ρ (kg/m ³)	C_p (J/kgK)
H ₂ O	0.613	997.1	4179
Al ₂ O ₃	40	3970	765
Cu	400	8933	385

Table 2. The alumina–copper/water (Al₂O₃–Cu/H₂O) correlation coefficient (Takabi and Salehi [43]; Ghalambaz et al. [44]).

Properties	Al ₂ O ₃ –Cu/H ₂ O
Density	$\rho_{hnf} = (1 - \phi_{hnf})\rho_f + \phi_1\rho_{s1} + \phi_2\rho_{s2}$
Dynamic viscosity	$\mu_{hnf} = \mu_f / (1 - \phi_{hnf})^{2.5}$
Thermal capacity	$(\rho C_p)_{hnf} = (1 - \phi_{hnf})(\rho C_p)_f + \phi_1(\rho C_p)_{s1} + \phi_2(\rho C_p)_{s2}$
Thermal conductivity	$\frac{k_{hnf}}{k_f} = \left[\frac{(\phi_1 k_{s1} + \phi_2 k_{s2})}{\phi_{hnf}} + 2k_f + 2(\phi_1 k_{s1} + \phi_2 k_{s2}) - 2\phi_{hnf} k_f \right] / \left[\frac{(\phi_1 k_{s1} + \phi_2 k_{s2})}{\phi_{hnf}} + 2k_f - (\phi_1 k_{s1} + \phi_2 k_{s2}) + \phi_{hnf} k_f \right]$
Electrical conductivity	$\frac{\sigma_{hnf}}{\sigma_f} = \left[\frac{(\phi_1 \sigma_{s1} + \phi_2 \sigma_{s2})}{\phi_{hnf}} + 2\sigma_f + 2(\phi_1 \sigma_{s1} + \phi_2 \sigma_{s2}) - 2\phi_{hnf} \sigma_f \right] / \left[\frac{(\phi_1 \sigma_{s1} + \phi_2 \sigma_{s2})}{\phi_{hnf}} + 2\sigma_f - (\phi_1 \sigma_{s1} + \phi_2 \sigma_{s2}) + \phi_{hnf} \sigma_f \right]$

The following similarity variables are implemented (Zainal et al. [8]; Fang and Jing [50]):

$$\psi(x, y, t) = \sqrt{\frac{u_0 v_f}{(1 - \beta t)}} x f(\eta), \eta = \sqrt{\frac{u_0}{(1 - \beta t) v_f}} y, \theta(\eta) = \frac{T - T_\infty}{T_w - T_\infty}, \tag{5}$$

so that

$$u = \frac{u_0 x f'(\eta)}{(1 - \beta t)}, v = -\sqrt{\frac{u_0 v_f}{(1 - \beta t)}} f(\eta), v_w = -\sqrt{\frac{u_0 v_f}{(1 - \beta t)}} S, \tag{6}$$

where S is the mass flux parameter with $S < 0$ for injection and $S > 0$ for suction, respectively, while v_f is the base fluid kinematic viscosity. It is necessary to formulate the similarity variables because there exist three independent variables (x, y, t) in the mathematical formulation, which is difficult to solve. By using the similarity variables, the similarity solution is produced. The similarity solution can reduce the three independent variables (x, y, t) to only one variable (η) by using appropriate similarity transformations. Hence, the similarity transformations are employed to reduce the nonlinear partial differential equations together with their partial derivatives into ordinary differential equations. Finally, the simplified mathematical model is solved using the `bvp4c` function in MATLAB software.

Substituting Equations (5) and (6) into Equations (2) and (3), the following ordinary (similarity) differential equations is obtained:

$$\frac{\mu_{hnf}/\mu_f}{\rho_{hnf}/\rho_f} f''' + f f'' - f'^2 + 1 - \varepsilon \left(f' + \frac{\eta}{2} f'' + 1 \right) - \frac{\sigma_{hnf}/\sigma_f}{\rho_{hnf}/\rho_f} M (f' + 1) = 0, \tag{7}$$

$$\frac{\mu_{hnf}/\mu_f}{\rho_{hnf}/\rho_f} f''' + f f'' - f'^2 + 1 - \varepsilon \left(f' + \frac{\eta}{2} f'' + 1 \right) - \frac{\sigma_{hnf}/\sigma_f}{\rho_{hnf}/\rho_f} M (f' + 1) = 0, \tag{8}$$

$$f(0) = S, f'(0) = \lambda, \theta(0) = 1, f'(\eta) \rightarrow -1, \theta(\eta) \rightarrow 0 \text{ as } y \rightarrow \infty, \tag{9}$$

where $M = \sigma_f B / u_0 \rho_f$ is the magnetic coefficient where $B = B_0 \sqrt{1 - \beta t}$, $Pr = \mu_f C_p / k_f$, $\varepsilon = \beta / a$ represents the unsteadiness parameter, and δ is the coefficient of heat generation/absorption. Meanwhile, $Q_s = Q_0 / (1 - \beta t)$ where Q_0 is the initial value of the heat generation/absorption coefficient. The heat generation/absorption parameter is given by Q where $Q > 0$ and $Q < 0$ represents the heat generation and heat absorption, respectively. The physical quantities of concern are $C_f = \frac{\mu_{hnf}}{\rho_f u_\infty^2} \left(\frac{\partial u}{\partial y} \right)_{y=0}$ and $Nu_x = \frac{x k_{hnf}}{k_f (T_w - T_\infty)} \left(-\frac{\partial T}{\partial y} \right)_{y=0}$ which denote as the skin friction coefficient and the local Nusselt number, respectively. Thus, we have

$$Re_x^{1/2} C_f = \frac{\mu_{hnf}}{\mu_f} f''(0), Re_x^{-1/2} Nu_x = -\frac{k_{hnf}}{k_f} \theta'(0), \tag{10}$$

where $Re_x = u_0 x^2 / v_f (1 - \beta t)$.

3. Stability Analysis

By perceiving the efforts of Merkin [51] and Merrill et al. [52], a stability analysis is implemented since the occurrence of several solutions was established in the boundary value problem (7) and (8). Now, by introducing a new transformation variable, τ is proposed under the unsteady-state query, as follows (Waini et al. [53]; Zainal et al. [54]):

$$u = \frac{u_0 x}{1 - \beta t} \frac{\partial f}{\partial \eta}(\eta, \tau), v = -\sqrt{\frac{u_0 v_f}{1 - \beta t}} f(\eta, \tau), \theta = \frac{T - T_\infty}{T_w - T_\infty}, \tag{11}$$

$$\eta = y \sqrt{\frac{u_0}{v_f (1 - \beta t)}}, \tau = \frac{u_0 t}{1 - \beta t}$$

Employing (11) into Equations (7) and (8), the following equations are secured:

$$\frac{\mu_{hf}/\mu_f}{\rho_{hf}/\rho_f} \frac{\partial^3 f}{\partial \eta^3} + f \frac{\partial^2 f}{\partial \eta^2} - \left(\frac{\partial f}{\partial \eta}\right)^2 + 1 - \varepsilon \left(\frac{\partial f}{\partial \eta} + \frac{\eta}{2} \frac{\partial^2 f}{\partial \eta^2} + 1\right) - \frac{\sigma_{hf}/\sigma_f}{\rho_{hf}/\rho_f} M \left(\frac{\partial f}{\partial \eta} + 1\right) - \frac{\partial^2 f}{\partial \eta \partial \tau} = 0, \tag{12}$$

$$\frac{1}{Pr} \left(\frac{K_{hf}/K_f}{(\rho C_p)_{hf}/(\rho C_p)_f}\right) \frac{\partial^2 \theta}{\partial \eta^2} + f \frac{\partial \theta}{\partial \eta} - \frac{\partial f}{\partial \eta} \theta - \varepsilon \left(\theta + \frac{\eta}{2} \frac{\partial \theta}{\partial \eta}\right) + \delta \theta - \frac{\partial \theta}{\partial \tau} = 0, \tag{13}$$

with respect to

$$f(0, \tau) = S, \quad \frac{\partial f}{\partial \eta}(0, \tau) = \lambda, \quad \theta(0, \tau) = 1, \tag{14}$$

$$\frac{\partial f}{\partial \eta}(\eta, \tau) \rightarrow -1 \quad \theta(\eta, \tau) \rightarrow 0 \text{ as } \eta \rightarrow \infty.$$

To scrutinise the steady flow solutions stability, where $f(\eta) = f_0(\eta)$ and $\theta(\eta) = \theta_0(\eta)$, we introduced the following equations:

$$f(\eta, \tau) = f_0(\eta) + e^{-\omega \tau} F(\eta), \tag{15}$$

$$\theta(\eta, \tau) = \theta_0(\eta) + e^{-\omega \tau} H(\eta),$$

which is based on the work of Weidman et al. [55]. Here, $F(\eta)$ and $H(\eta)$ are relatively small to $f_0(\eta)$ and $\theta_0(\eta)$ whilst ω is the unidentified eigenvalue. The eigenvalue problem (12) and (13) leading to an infinite number of eigenvalues $\omega_1 < \omega_2 < \omega_3 \dots$ that disclose a steady flow and initial deterioration when ω_1 is positive. On the other hand, once ω_1 is found out negative; thus an initial development of perturbations is discovered. This finding exposed the occurrence of unstable flow.

Replacing Equations (15) into Equations (12) and (13), hence

$$\frac{\mu_{hf}/\mu_f}{\rho_{hf}/\rho_f} \frac{\partial^3 F}{\partial \eta^3} + f_0 \frac{\partial^2 F}{\partial \eta^2} + F \frac{\partial^2 f_0}{\partial \eta^2} - 2 \frac{\partial F}{\partial \eta} \frac{\partial f_0}{\partial \eta} - \varepsilon \left(\frac{\partial F}{\partial \eta} + \frac{\eta}{2} \frac{\partial^2 F}{\partial \eta^2}\right) - \frac{\sigma_{hf}/\sigma_f}{\rho_{hf}/\rho_f} M \left(\frac{\partial F}{\partial \eta}\right) + \omega \frac{\partial F}{\partial \eta} = 0, \tag{16}$$

$$\frac{1}{Pr} \left(\frac{K_{hf}/K_f}{(\rho C_p)_{hf}/(\rho C_p)_f}\right) \frac{\partial^2 H}{\partial \eta^2} + f_0 \frac{\partial H}{\partial \eta} + F \frac{\partial \theta_0}{\partial \eta} - \left(H \frac{\partial f_0}{\partial \eta} + \theta_0 \frac{\partial F}{\partial \eta}\right) - \varepsilon \left(H + \frac{\eta}{2} \frac{\partial H}{\partial \eta}\right) + (\delta + \omega)H = 0, \tag{17}$$

with respect to

$$F(0) = 0, \quad \frac{\partial F}{\partial \eta}(0) = 0, \quad H(0) = 0, \tag{18}$$

$$\frac{\partial F}{\partial \eta}(\eta) \rightarrow 0, \quad H(\eta) \rightarrow 0 \text{ as } \eta \rightarrow \infty.$$

The steady-state flow solutions, i.e., $f_0(\eta)$ and $\theta_0(\eta)$ were implemented via $\tau \rightarrow 0$. Eventually, the solution to the linearised eigenvalue problem is identified

$$\frac{\mu_{hf}/\mu_f}{\rho_{hf}/\rho_f} F''' + \left(f_0 - \varepsilon \frac{\eta}{2}\right) F'' - \left(2f_0' + \varepsilon + \omega + \frac{\sigma_{hf}/\sigma_f}{\rho_{hf}/\rho_f} M\right) F' + f_0'' F = 0, \tag{19}$$

$$\frac{1}{Pr} \left(\frac{K_{hf}/K_f}{(\rho C_p)_{hf}/(\rho C_p)_f}\right) H'' + \left(f_0 - \varepsilon \frac{\eta}{2}\right) H' - (f_0' + \varepsilon - \delta - \omega)H - \theta_0 F' + \theta_0' F = 0, \tag{20}$$

$$F(0, \tau) = 0, \quad F'(0, \tau) = 0, \quad H(0, \tau) = 0, \tag{21}$$

$$F'(\eta) \rightarrow 0, \quad G(\eta) \rightarrow 0 \text{ as } \eta \rightarrow \infty.$$

According to [56], the possible eigenvalues can be established by relaxing a boundary condition. Here, the value of $F'(\eta) \rightarrow 0$ is fixed as $\eta \rightarrow \infty$, thus the linearised eigenvalue problems (19) and (20) are exposed as $F''(0) = 1$ when ω_1 is set up.

4. Results and Discussion

The resulting ordinary differential equations expressed in Equations (7)–(9) is clarified by employing the `bvp4c` tool in the MATLAB software. In this technique, the essential

approximation of boundary layer thickness is critical while discovering multiple solutions. Before achieving the required outcome, several attempts need to be performed in offering a significant initial prediction. The reliability of the results is evaluated with Turkiymazoglu et al. [19] and Bhattacharyya [57] as accessible in Table 3. The authors discovered that the current findings are remarkably consistent with previous work. Thus, we are certain that the suggested conceptual model can effectively investigate the heat transfer and fluid flow activities.

Table 3. Approximation values of $Re_x^{1/2}C_f$ by certain values of λ when $\varepsilon = M = \delta = S = \phi_1 = \phi_2 = 0$.

λ	Present Result		Turkiymazoglu et al. [19]		Bhattacharyya [57]	
	First Solution	Second Solution	First Solution	Second Solution	First Solution	Second Solution
−0.25	1.4022408	-	1.4022408	-	1.4022405	-
−0.50	1.4956698	-	1.4956670	-	1.4956697	-
−0.75	1.4892982	-	1.4892982	-	1.4892981	-
−1.00	1.3288169	0.0000000	1.3288168	0.0000000	1.3288169	0.0000000
−1.15	1.0822312	0.1167021	1.0822312	0.1167021	1.0822316	0.1167023
−1.20	0.9324733	0.2336497	0.9324733	0.2336497	0.9324728	0.2336491
−1.2465	0.5842817	0.5542962	0.5842813	0.5542947	0.5842915	0.5542856
−1.24657	0.5745257	0.5640125	0.5774525	0.5640081	0.5745268	0.5639987

The numerical calculations for different physical parameters used in the study were performed. In this study, a variety of ϕ_2 is implemented ($0.00 \leq \phi_2 \leq 0.02$), while $\phi_1 = 0.01$. Certain limiting parameters are utilised to assure the accuracy of the outputs, and they are fixed to the extents listed here; $4.0 \leq M \leq 6.0$ and $0.0 \leq \delta \leq 1.5$ to guarantee that the obtained solutions are compatible. It should be noted that, in order to achieve the required solution, an appropriate preliminary estimation should be determined by the values of the specified parameter.

The effect of the selected parameter towards $Re_x^{1/2}C_f$ and $Re_x^{-1/2}Nu_x$ when $Pr = 6.2$, $\phi_1 = 0.01$, $S = 6.0$ and $\lambda = -10$ for various values of ϕ_2 , M and δ is presented in Table 4. The increment values of ϕ_2 and M are reported to significantly improve the values of $Re_x^{1/2}C_f$, while the increment values of δ reduced the values of $Re_x^{-1/2}Nu_x$, as displayed in Table 4. As there exist dual solutions in this study, performing a stability analysis is needed. The first solution is usually denoted reliable because it fulfils the far-field boundary condition; however, by conducting a stability analysis, we are able to confirm the accurate and reliable solutions convincingly. In the stability analysis procedure, the smallest eigenvalue ω_1 indicates the characteristics of the dual solutions. When ω_1 is positive, the flow is considered stable since the solutions comply with the stabilising property where an initial decay is permitted. When ω_1 is negative, however, the flow is considered unstable because it causes an initial development of disturbances. The first solution was found to be reliable due to its positive value, as witnessed in Table 5, while the second solution is unreliable.

The preparation of compatible conventional/hybrid nanofluids is required to analyse nanofluid flow characteristics and heat transfer effectiveness. The goal of developing stable nanofluids was to improve the thermal properties of working fluids while using as few nanoparticles as possible, as reported by Arifin et al. [58]. Suresh et al. [59], on the other hand, worked on the synthesis of nanocomposite Al_2O_3 -Cu/ H_2O powder and its properties at different volume concentrations. According to their research, nanofluid stability decreases as volume concentration rises.

Table 4. Values of $Re_x^{1/2}C_f$ and $Re_x^{-1/2}Nu_x$ for Al_2O_3 -Cu/water hybrid nanofluid when $Pr = 6.2, \phi_1 = 0.01, S = 6.0$ and $\lambda = -10$ for various values of ϕ_2, M and δ .

ϕ_2	M	δ	Al ₂ O ₃ -Cu/Water Hybrid Nanofluid ($\phi_1 = 0.01$)	
			$Re_x^{1/2}C_f$	$Re_x^{-1/2}Nu_x$
0.00	6.0	0.5	41.0286336560	33.2812323540
0.01			44.4794570250	33.1259684480
0.02			47.9973405430	32.9737922260
0.01	4.0		35.4463147500	33.0027615510
	5.0		40.9347604490	33.0792778990
	6.0		44.4794570250	33.1259684480
		0.0	-	33.2417593770
		0.5	-	33.1259684480
		1.0	-	33.0091507970

Table 5. The smallest eigenvalues ω_1 with assorted λ .

λ	First Solution ω_1	Second Solution ω_1
-10	2.0570	-1.8571
-10.3	0.4956	-0.4836
-10.31	0.3416	-0.3359
-10.318	0.2560	-0.2527
-10.3183	0.2001	-0.1981
-10.3185	0.1210	-0.1203

The impact of nanoparticles concentration when ϕ_2 varied is described in Figures 2–5, while the value of alumina is fixed at $\phi_1 = 0.1$ as the sheet shrinks. Figures 2 and 3 show the characteristic of the skin friction coefficient ($f''(0)$) and the velocity profiles ($f'(\eta)$) as the sheet shrinks. The addition of ϕ_2 clearly enhances the $f''(0)$ tendency from Al_2O_3/H_2O nanofluid to Al_2O_3 -Cu/ H_2O hybrid nanofluid, as displayed in Figure 2. The result indicates that as $f''(0)$ increases, the frictional drag exerted upsurges and potentially slowing the boundary layer separation on the shrinking surface of Al_2O_3 -Cu/ H_2O hybrid nanofluid. The velocity profiles in Figure 3 show a declining trend for the first solution, but a reversal trend for the second solution is observed.

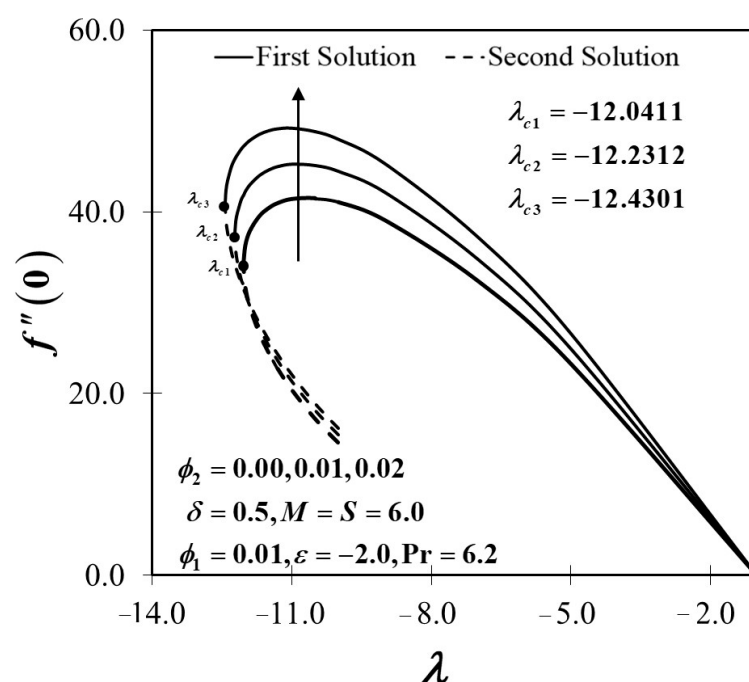


Figure 2. $f''(0)$ against λ by various ϕ_2 .

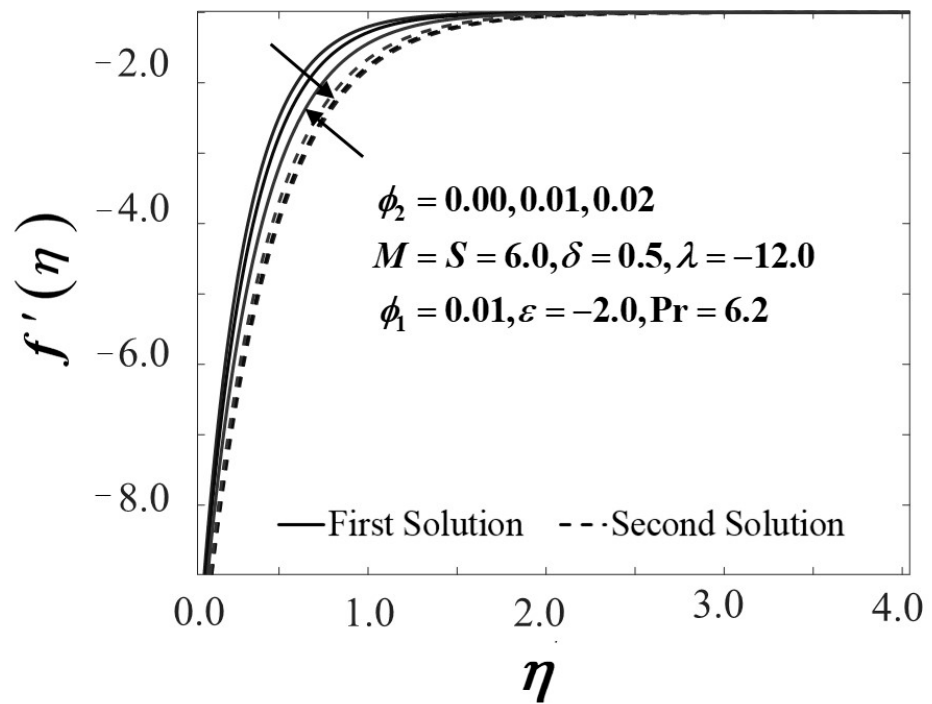


Figure 3. $f'(\eta)$ with various ϕ_2 when $\lambda = -12.0$.

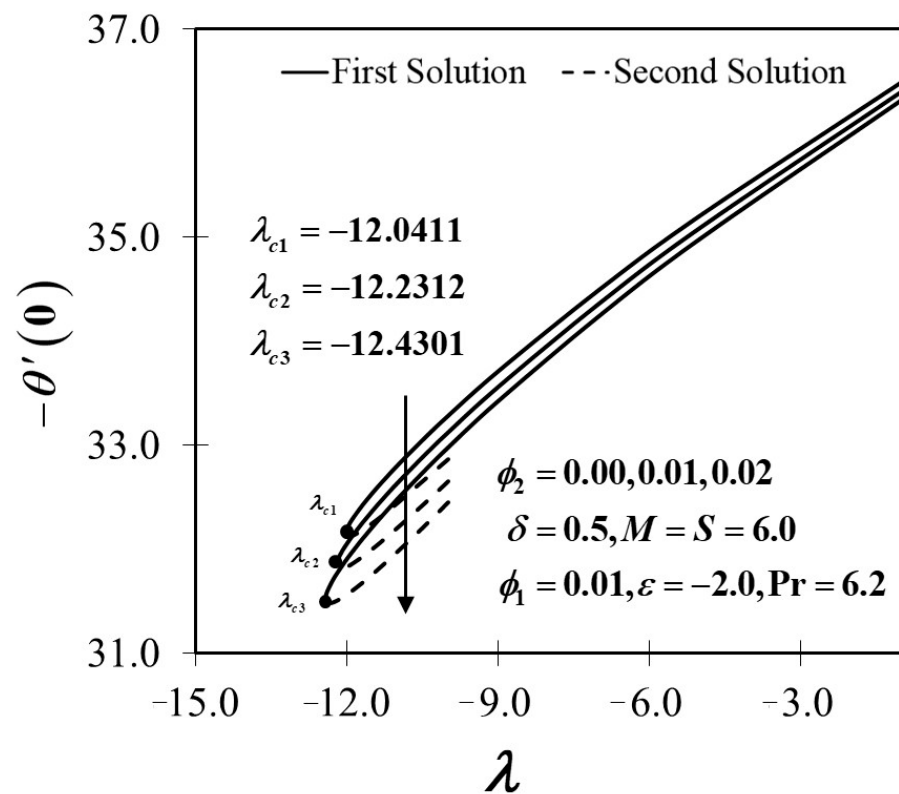


Figure 4. $-\theta'(0)$ against λ by various ϕ_2 .

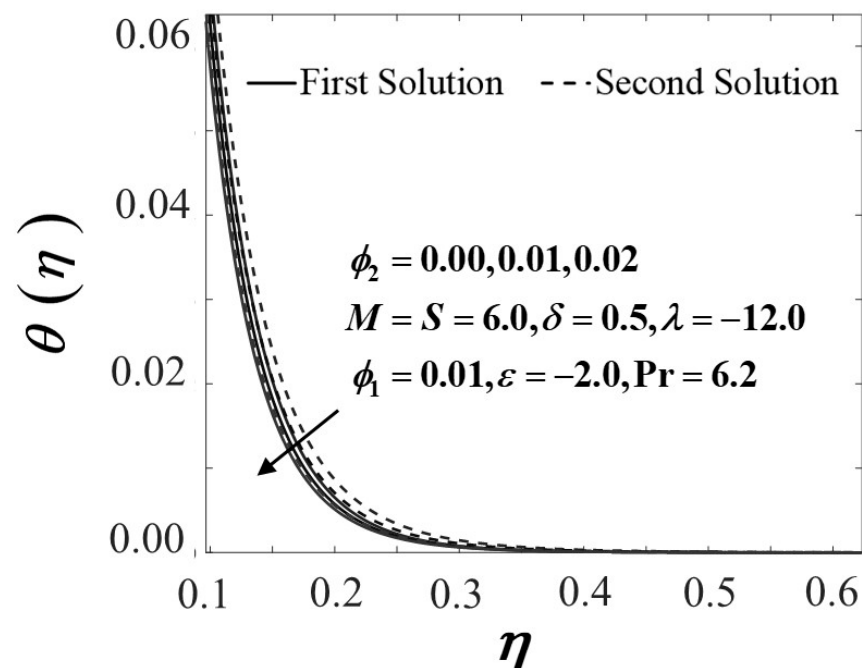


Figure 5. $\theta(\eta)$ with various ϕ_2 when $\lambda = -12.0$.

Meanwhile, Figure 4 describes the reduction in $-\theta'(0)$ results to an increase in ϕ_2 . The heat transfer activity in $\text{Al}_2\text{O}_3\text{-Cu}/\text{H}_2\text{O}$ hybrid nanofluid was noticeably slowed by a larger value of nanoparticle volume concentration. In other words, when the mass of the $\text{Al}_2\text{O}_3\text{-Cu}/\text{H}_2\text{O}$ hybrid nanoparticles increases, the temperature of the decreasing sheet rises, reducing the heat transfer rate. The temperature profiles or $\theta(\eta)$ reveals a reduction trend in both solutions. This may have occurred due to the simultaneous development of the suction parameter and nanoparticle volume fraction.

It is widely known that the Lorentz force in transport phenomena has a significant impact on fluid and heat transfer behaviour. The Lorentz force, which is heavily affected by the electromagnetic force, tends to drag the fluid velocity down. As a result, the temperature field of the working fluid increases. The findings in Figures 6–9 support this argument which is discussed in detail afterwards. Figures 6 and 7 exemplify the trend of $f''(0)$ and $f'(\eta)$ for an escalation of the magnetic parameter M . The findings reveal that higher values of M aggravate the skin friction coefficient $f''(0)$ while, the velocity profile $f'(\eta)$ of the first solution displays a reduction in the momentum boundary layer thickness, as M intensifies in the shrinking case. Conversely, the momentum boundary layer thickness in the second solution increases as the magnetic parameter is added, resulting in a reversal of the velocity profile pattern. The performance of heat transfers $-\theta'(0)$ and the thermal profile $\theta(\eta)$ in the influence of M is examined in Figures 8 and 9. It is found that the appearance of M has a particular influence on the fluid temperature. Substantially, $-\theta'(0)$ boosts when the magnetic parameter is intensified (see Figure 8) attributed to the existence of the Lorentz force, as discussed earlier. The fluid temperature can also disperse from the surface to the flow owing to this force. This can be seen in the temperature distribution profile shown in Figure 9. The development and transmission of the drag force into the flow helps to increase the temperature field, which ultimately increases the thermal boundary layer thickness. In this particular study, the authors can deduce that the addition of the magnetic parameter supports a substantial improvement in heat transfer performance from the current and existing evidence. Even so, the authors would like to point out that when different control parameters are taken into account, the effects may differ.

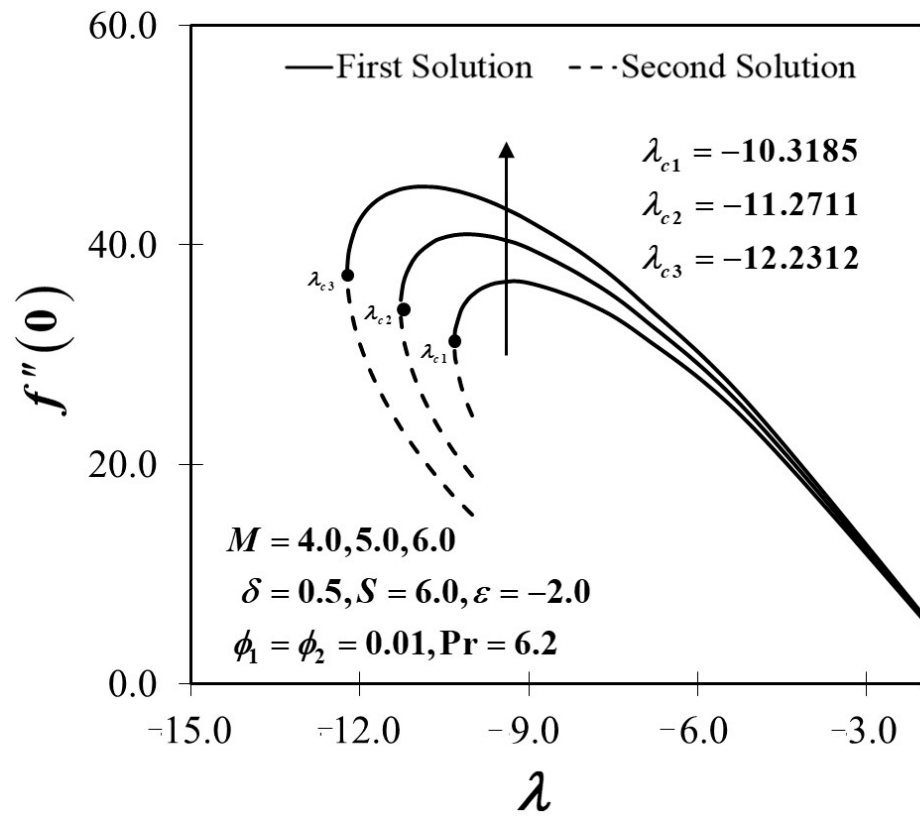


Figure 6. $f''(0)$ against λ by various M .

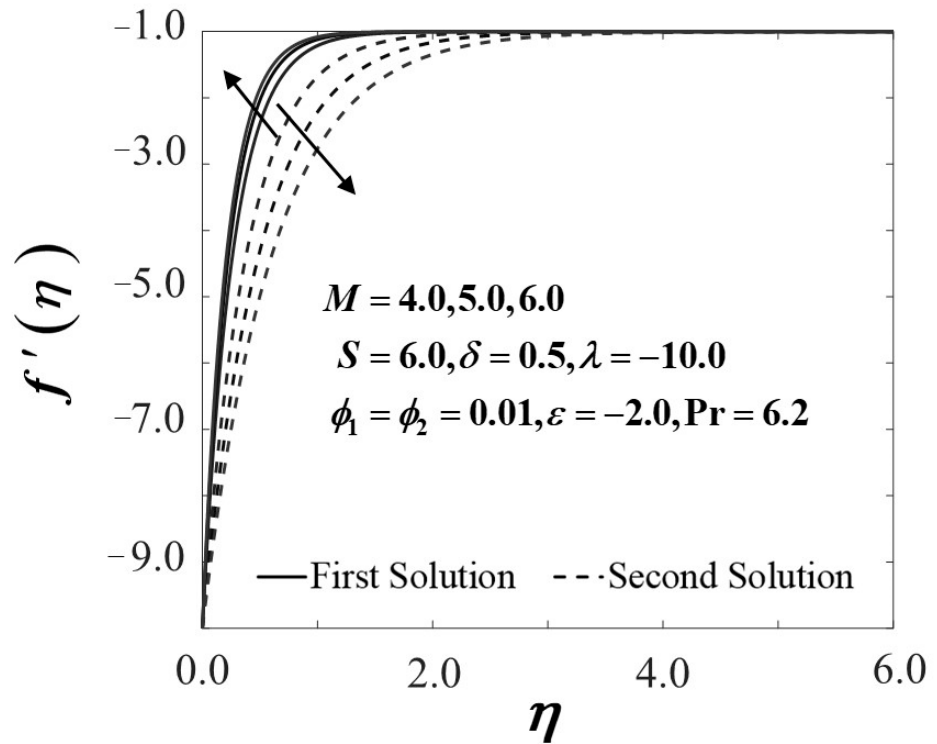


Figure 7. $f'(\eta)$ with various M when $\lambda = -10.0$.

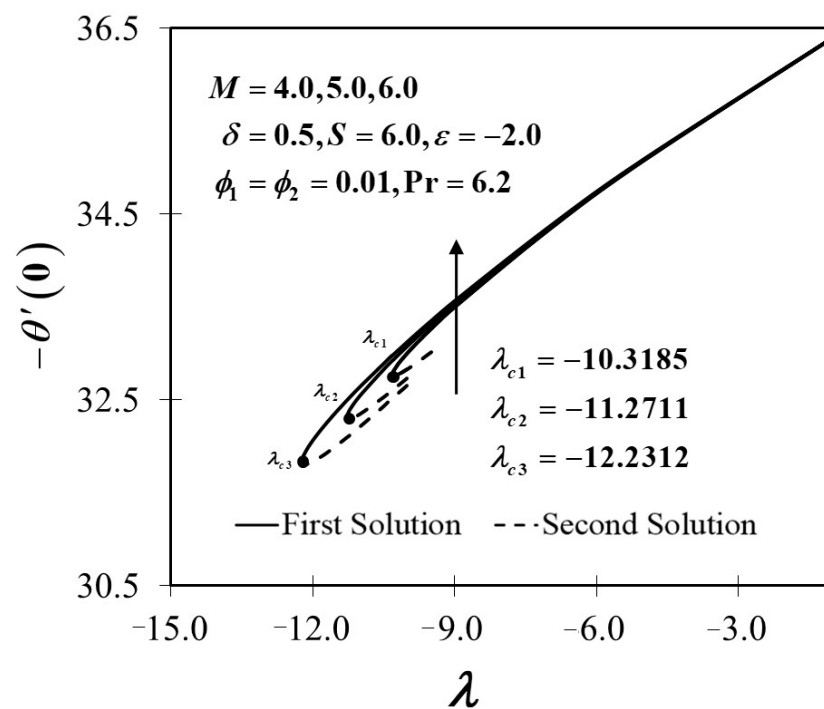


Figure 8. $-\theta'(0)$ against λ by various M .

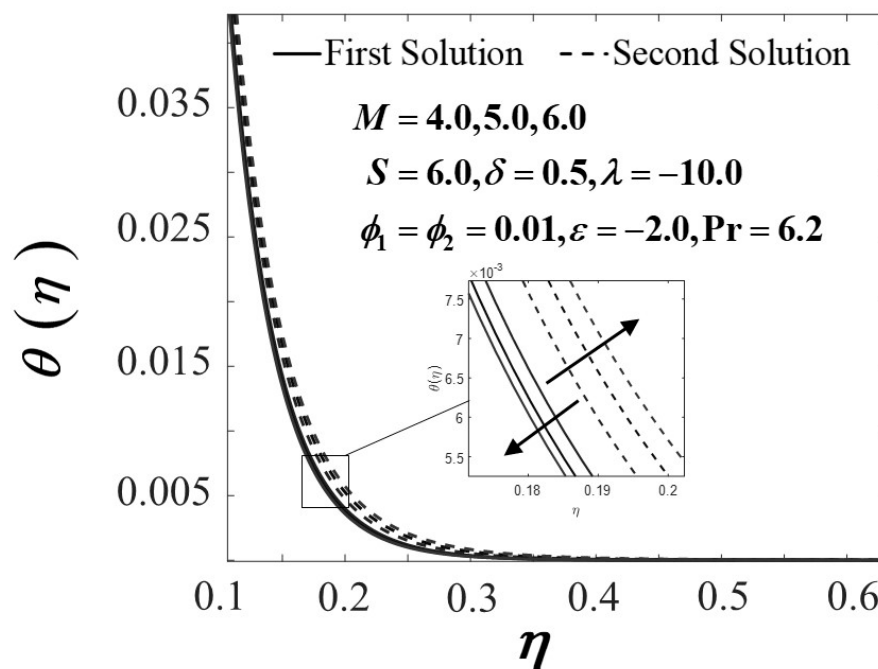


Figure 9. $\theta(\eta)$ with various M when $\lambda = -10.0$.

In general, the temperature field of $\text{Al}_2\text{O}_3\text{-Cu}/\text{H}_2\text{O}$ hybrid nanofluid will be physically improved by including the heat generation/absorption parameter, while the sheet shrinks due to the production of thermal energy at the boundary layer. Figure 10 demonstrates the temperature distribution profiles $\theta(\eta)$ of the working fluid with various values of δ . As exhibited in Figure 10, the thickness of the thermal boundary layer in the shrinking sheet grows when the heat generation ($\delta > 0$) parameter is amplified. The temperature in the boundary layer, in particular, increases as a result of heat generation ($\delta > 0$). It is indeed worth noting that the fluid temperature peak occurs near the wall rather than on the wall at greater heat generation values. From a physical standpoint, the increase in

fluid temperature is caused by the inclusion of heat generation. This phenomenon explains the growth of the thermal boundary layer thickness. The observations in the previous analyses (see Zainal et al. [48], Hayat and Nadeem [60]) indicate the same effects with the current findings.

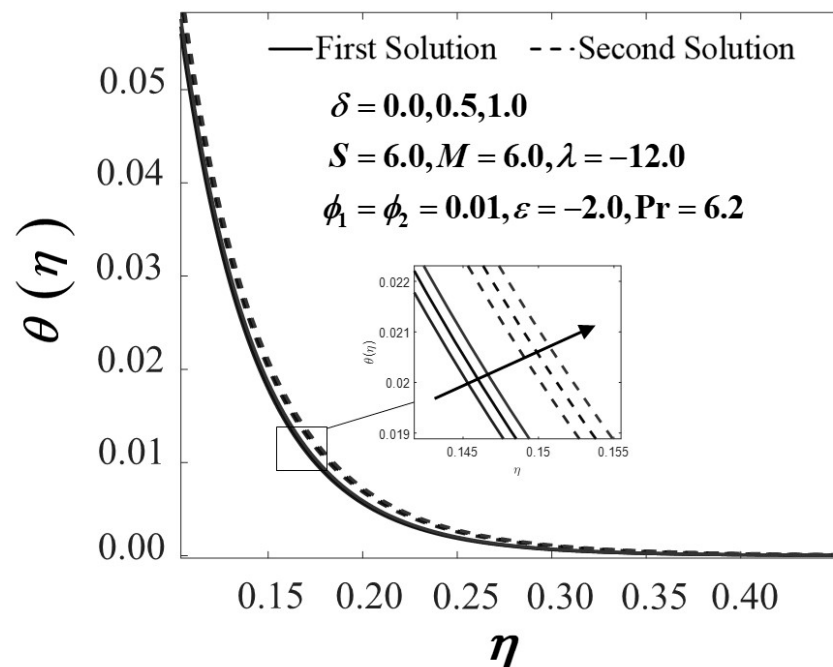


Figure 10. $\theta(\eta)$ with $\delta = 0.0, 0.5, 1.0$.

5. Conclusions

Mathematical analysis on unsteady MHD rear stagnation point flow with a heat generation/absorption effect in $\text{Al}_2\text{O}_3\text{-Cu}/\text{H}_2\text{O}$ hybrid nanofluid was validated numerically in the present study. The impact of assorted operating parameters, for example, the volume fraction of nanoparticle, the MHD and heat generation/absorption parameter, were scrutinised. The outcomes suggest that dual solutions are feasible across the $\text{Al}_2\text{O}_3\text{-Cu}/\text{H}_2\text{O}$ hybrid nanofluid is verifiable in certain controlling parameters. However, the dual solutions occur when the sheet is shrinking. The stability analysis enables us to permit our first solution consistency, while the second solution is considered unstable. Moreover, when the magnetic parameter is induced in the operating fluid, the heat transfer performance is increased. The inclusion of the nanoparticle volume fraction enhances the skin friction coefficient in $\text{Al}_2\text{O}_3\text{-Cu}/\text{H}_2\text{O}$ hybrid nanofluid but declines the local Nusselt number. A recent aggregation to the heat generation factor value has donated to the development in the temperature distribution profile. As a result, the thermal boundary layer is urged to elevate, and the heat transfer performance is degraded accordingly.

Author Contributions: Article preparation, N.A.Z.; formulation and methodology, N.A.Z., R.N., K.N., and I.P.; research design, N.A.Z., R.N., K.N., and I.P.; analysis of result, N.A.Z., R.N., and K.N.; validation, R.N. and K.N.; review and editing, N.A.Z., R.N., K.N., and I.P. All authors have read and agreed to the published version of the manuscript.

Funding: This project is funded by GUP-2019-034 from Universiti Kebangsaan Malaysia.

Institutional Review Board Statement: Not applicable.

Informed Consent Statement: Not applicable.

Data Availability Statement: Not applicable.

Acknowledgments: All authors value the useful input from knowledgeable reviewers.

Conflicts of Interest: The authors declare no conflict of interest.

References

1. Katagiri, M. On the separation of magnetohydrodynamic flow near the rear stagnation point. *J. Phys. Soc. Jpn.* **1969**, *27*, 1045–1050. [[CrossRef](#)]
2. Mitrishkin, Y.V.; Korenev, P.S.; Kartsev, N.M.; Kuznetsov, E.A.; Prokhorov, A.A.; Patrov, M.I. Plasma magnetic cascade multiloop control system design methodology in a tokamak. *Control Eng. Pract.* **2019**, *87*, 97–110. [[CrossRef](#)]
3. Mitryushkin, Y.V.; Korenev, P.S.; Prokhorov, A.A.; Kartsev, N.M.; Patrov, M.I. Plasma Control in Tokamaks. Part 1. *Adv. Syst. Sci. Appl.* **2018**, *18*, 26–52.
4. De Tommasi, G. Plasma magnetic control in tokamak devices. *J. Fusion Energy* **2019**, *38*, 406–436. [[CrossRef](#)]
5. Hartmann, J. Hg-Dynamics I: Theory of the laminar conductive liquid in a homogeneous magnetic field. *K. Dan. Vidensk. Selsk. Mat. Fys. Medd.* **1937**, *15*, 1–28.
6. Leibovich, S. Magnetohydrodynamic flow at a rear stagnation point. *J. Fluid Mech.* **1967**, *29*, 401–413. [[CrossRef](#)]
7. Pavlov, K.B. Magnetohydrodynamic flow of an incompressible viscous fluid caused by deformation of a plane surface. *Magn. Gidrodin.* **1974**, *4*, 146–147.
8. Zainal, N.A.; Nazar, R.; Naganthran, K.; Pop, I. Unsteady MHD stagnation point flow-induced stretching/shrinking sheet of hybrid nanofluid by exponentially permeable. *Eng. Sci. Technol. Int. J.* **2021**, *24*, 1201–1210.
9. Versaci, M.; Cutrupi, A.; Palumbo, A. A magneto-thermo-static study of a magneto-rheological fluid damper: A finite element analysis. *IEEE Trans. Magn.* **2020**, *57*, 1–10. [[CrossRef](#)]
10. Seth, G.S.; Bhattacharyya, A.; Kumar, R.; Chamkha, A.J. Entropy generation in hydromagnetic nanofluid flow over a non-linear stretching sheet with Navier's velocity slip and convective heat transfer. *Phys. Fluids* **2018**, *30*, 122003. [[CrossRef](#)]
11. Aslani, K.E.; Sarris, I.E. Effect of micromagnetorotation on magnetohydrodynamic Poiseuille micropolar flow: Analytical solutions and stability analysis. *J. Fluid Mech.* **2021**, *920*, A25. [[CrossRef](#)]
12. Hiemenz, K. Die Grenzschicht an einem in den gleichförmigen Flüssigkeitsstrom eingetauchten geraden Kreiszyylinder. *Dinglers Polytech J.* **1911**, *326*, 321–324.
13. Homann, F. Der Einfluss grosser Zähigkeit bei der Strömung um den Zylinder und um die Kugel. *Z. Angew. Math. Mech.* **1936**, *16*, 153–164. [[CrossRef](#)]
14. Rauwendaal, C. *Polymer Extrusion*; Hanser Publications: Cincinnati, OH, USA, 1985.
15. Fisher, E.G. *Extrusion of Plastics*; Wiley: New York, NY, USA, 1976.
16. Proudman, I.; Johnson, K. Boundary-layer growth near a rear stagnation point. *J. Fluid Mech.* **1961**, *12*, 161–168. [[CrossRef](#)]
17. Robins, A.; Howarth, J.A. Boundary-layer development at a two-dimensional rear stagnation point. *J. Fluid Mech.* **1972**, *56*, 161–171. [[CrossRef](#)]
18. Howarth, J.A. A note on boundary-layer growth at a three-dimensional rear stagnation point. *J. Fluid Mech.* **1973**, *59*, 769–773. [[CrossRef](#)]
19. Turkyilmazoglu, M.; Naganthran, K.; Pop, I. Unsteady MHD rear stagnation point flow over off-centred deformable surfaces. *Int. J. Numer. Methods Heat Fluid Flow.* **2017**, *27*, 1554–1570. [[CrossRef](#)]
20. Khashi'ie, N.S.; Hafidzuddin, E.H.; Arifin, N.M.; Wahi, N. Stagnation point flow of hybrid nanofluid over a permeable vertical stretching/shrinking cylinder with thermal stratification effect. *CFD Lett.* **2020**, *12*, 80–94.
21. Khashi'ie, N.S.; Arifin, N.M.; Merkin, J.H.; Yahaya, R.I.; Pop, I. Mixed convective stagnation point flow of a hybrid nanofluid toward a vertical cylinder. *Int. J. Numer. Methods Heat Fluid Flow.* **2021**, in press. [[CrossRef](#)]
22. Zainal, N.A.; Nazar, R.; Naganthran, K.; Pop, I. Unsteady EMHD stagnation point flow over a stretching/shrinking sheet in a hybrid Al₂O₃-Cu/H₂O nanofluid. *Int. Commun. Heat Mass Transf.* **2021**, *123*, 105205. [[CrossRef](#)]
23. Zainal, N.A.; Nazar, R.; Naganthran, K.; Pop, I. Unsteady MHD mixed convection flow in hybrid nanofluid at three-dimensional stagnation point. *Mathematics* **2021**, *9*, 549. [[CrossRef](#)]
24. Smith, F.T. Steady and unsteady boundary layer separation. *Annu. Rev. Fluid Mech.* **1986**, *18*, 197–220. [[CrossRef](#)]
25. White, F.M. *Viscous Fluid Flow*, 2nd ed.; McGraw-Hill: New York, NY, USA, 1991.
26. McCroskey, W.J. Some current research in unsteady fluid dynamics—The 1976 Freeman Scholar Lecture, Trans. ASME. *J. Fluid Eng.* **1977**, *99*, 8–39. [[CrossRef](#)]
27. Benson, R.S.; Garg, R.D.; Woollatt, D. A numerical solution of unsteady flow problems. *Int. J. Mech. Sci.* **1964**, *6*, 117–144. [[CrossRef](#)]
28. Sears, W.R.; Telionis, D.P. Boundary-layer separation in unsteady flow. *SIAM J. Appl. Math.* **1975**, *28*, 215–235. [[CrossRef](#)]
29. Hayat, T.; Imtiaz, M.; Alsaedi, A. Unsteady flow of nanofluid with double stratification and magnetohydrodynamics. *Int. J. Heat Mass Transf.* **2016**, *92*, 100–109. [[CrossRef](#)]
30. Jahan, S.; Sakidin, H.; Nazar, R.; Pop, I. Unsteady flow and heat transfer past a permeable stretching/shrinking sheet in a nanofluid: A revised model with stability and regression analyses. *J. Mol. Liq.* **2018**, *261*, 550–564. [[CrossRef](#)]
31. Zainal, N.A.; Nazar, R.; Naganthran, K.; Pop, I. Unsteady three-dimensional MHD non-axisymmetric Homann stagnation point flow of a hybrid nanofluid with stability analysis. *Mathematics* **2020**, *8*, 784. [[CrossRef](#)]
32. Hafidzuddin, M.E.H.; Nazar, R.; Arifin, N.M.; Pop, I. Unsteady flow and heat transfer over a permeable stretching/shrinking sheet with generalised slip velocity. *Int. J. Numer. Methods Heat Fluid Flow* **2018**, *28*, 1457–1470. [[CrossRef](#)]

33. Subhani, S.M.; Nadeem, Numerical investigation of unsteady MHD flow of micropolar hybrid nanofluid in porous medium. *Phys. Scr.* **2019**, *94*, 105220. [[CrossRef](#)]
34. Khan, U.; Waini, I.; Ishak, A.; Pop, I. Unsteady hybrid nanofluid flow over a radially permeable shrinking/stretching surface. *J. Mol. Liq.* **2021**, *331*, 115752. [[CrossRef](#)]
35. Waini, I.; Ishak, A.; Pop, I. Unsteady hybrid nanofluid flow on a stagnation point of a permeable rigid surface. *ZAMM—J. Appl. Math. Mech./Z. Angew. Math. Mech.* **2020**, *101*, e202000193.
36. Rahman, M.M.; Sattar, M.A. Magneto hydrodynamic convective flow of a micropolar fluid past a continuously moving vertical porous plate in the presence of heat generation/absorption. *J. Heat Transf.* **2006**, *128*, 142–152. [[CrossRef](#)]
37. Vajravelu, K.; Hadjinicolaou, A. Heat transfer in a viscous fluid over a stretching sheet with viscous dissipation and internal heat generation. *Int. Commun. Heat Mass Transf.* **1993**, *20*, 417–430. [[CrossRef](#)]
38. Alsaedi, A.; Awais, M.; Hayat, T. Effects of heat generation/absorption on stagnation point flow of nanofluid over a surface with convective boundary conditions. *Commun. Nonlinear Sci. Numer. Simul.* **2012**, *17*, 4210–4223. [[CrossRef](#)]
39. Soomro, F.A.; Haq, R.U.; Al-Mdallal, Q.M.; Zhang, Q. Heat generation/absorption and nonlinear radiation effects on stagnation point flow of nanofluid along a moving surface. *Results Phys.* **2018**, *8*, 404–414. [[CrossRef](#)]
40. Jo, E.; Park, J.H.; Park, J.; Hwang, J.; Chung, K.Y.; Nam, K.W.; Kim, S.M.; Chang, W. Different thermal degradation mechanisms: Role of aluminum in Ni-rich layered cathode materials. *Nano Energy* **2020**, *78*, 105367. [[CrossRef](#)]
41. Berni, F.; Fontanesi, S. A 3D-CFD methodology to investigate boundary layers and assess the applicability of wall functions in actual industrial problems: A focus on in-cylinder simulations. *Appl. Therm. Eng.* **2020**, *174*, 115320. [[CrossRef](#)]
42. Tiwari, R.K.; Das, M.K. Heat transfer augmentation in a two-sided lid-driven differentially heated square cavity utilising nanofluids. *Int. J. Heat Mass Transf.* **2007**, *50*, 2002–2018. [[CrossRef](#)]
43. Takabi, B.; Salehi, S. Augmentation of the heat transfer performance of a sinusoidal corrugated enclosure by employing hybrid nanofluid. *Adv. Mech. Eng.* **2014**, *6*, 147059. [[CrossRef](#)]
44. Ghalambaz, M.; Ros, N.C.; Ros, A.V.; Pop, I. Mixed convection and stability analysis of stagnation-point boundary layer flow and heat transfer of hybrid nanofluids over a vertical plate. *Int. J. Numer. Methods Heat Fluid Flow.* **2019**, *30*, 3737–3754. [[CrossRef](#)]
45. Babu, J.R.; Kumar, K.K.; Rao, S.S. State-of-art review on hybrid nanofluids. *Renew. Sustain. Energy Rev.* **2017**, *77*, 551–565. [[CrossRef](#)]
46. Hussain, S.; Ahmed, S.E.; Akbar, T. Entropy generation analysis in MHD mixed convection of hybrid nanofluid in an open cavity with a horizontal channel containing an adiabatic obstacle. *Int. J. Heat Mass Transf.* **2017**, *114*, 1054–1066. [[CrossRef](#)]
47. Devi, S.S.U.; Devi, S.A. Numerical investigation of three-dimensional hybrid Cu–Al₂O₃/water nanofluid flow over a stretching sheet with effecting Lorentz force subject to Newtonian heating. *Can. J. Phys.* **2016**, *94*, 490–496. [[CrossRef](#)]
48. Zainal, N.A.; Nazar, R.; Naganthran, K.; Pop, I. Heat generation/absorption effect on MHD flow of hybrid Nnanofluid over bidirectional exponential stretching/shrinking sheet. *Chin. J. Phys.* **2021**, *69*, 118–133. [[CrossRef](#)]
49. Abu-Nada, E.; Oztop, H.F. Effects of inclination angle on natural convection in enclosures filled with Cu-water nanofluid. *Int. J. Heat Fluid Flow.* **2009**, *30*, 669–678. [[CrossRef](#)]
50. Fang, T.; Jing, W. Closed-form analytical solutions of flow and heat transfer for an unsteady rear stagnation-point flow. *Int. J. Heat Mass Transf.* **2013**, *62*, 55–62. [[CrossRef](#)]
51. Merkin, J.H. Mixed convection boundary layer flow on a vertical surface in a saturated porous medium. *J. Eng. Math.* **1980**, *14*, 301–313. [[CrossRef](#)]
52. Merrill, K.; Beauchesne, M.; Previte, J.; Poullet, J.; Weidman, P. Final steady flow near a stagnation point on a vertical surface in a porous medium. *Int. J. Heat Mass Transf.* **2006**, *49*, 4681–4686. [[CrossRef](#)]
53. Waini, I.; Ishak, A.; Pop, I. Unsteady flow and heat transfer past a stretching/shrinking sheet in a hybrid nanofluid. *Int. J. Heat Mass Transf.* **2019**, *136*, 288–297. [[CrossRef](#)]
54. Zainal, N.A.; Nazar, R.; Naganthran, K.; Pop, I. Stability analysis of MHD hybrid nanofluid flow over a stretching/shrinking sheet with quadratic velocity. *Alex. Eng. J.* **2020**, *60*, 915–926. [[CrossRef](#)]
55. Weidman, P.D.; Kubitschek, D.G.; Davis, A.M.J. The effect of transpiration on self-similar boundary layer flow over moving surfaces. *Int. J. Eng. Sci.* **2006**, *44*, 730–737. [[CrossRef](#)]
56. Harris, S.D.; Ingham, D.B.; Pop, I. Mixed convection boundary-layer flow near the stagnation point on a vertical surface in a porous medium: Brinkman model with slip. *Transp. Porous Media* **2009**, *77*, 267–285. [[CrossRef](#)]
57. Bhattacharyya, K. Dual solutions in boundary layer stagnation-point flow and mass transfer with chemical reaction past a stretching/shrinking sheet. *Int. Commun. Heat Mass Transf.* **2011**, *38*, 917–922. [[CrossRef](#)]
58. Arifin, N.M.; Nazar, R.; Pop, I. Non-Isobaric Marangoni boundary layer flow for Cu, Al₂O₃ and TiO₂ nanoparticles in a water-based fluid. *Meccanica* **2011**, *46*, 833–843. [[CrossRef](#)]
59. Suresh, S.; Venkataraj, K.P.; Selvakumar, P. Synthesis, characterisation of Al₂O₃-Cu nanocomposite powder and water-based nanofluids. *Adv. Mater. Res.* **2011**, *328*, 1560–1567. [[CrossRef](#)]
60. Hayat, T.; Nadeem, S. Heat transfer enhancement with Ag–CuO/water hybrid nanofluid. *Results Phys.* **2017**, *7*, 2317–2324. [[CrossRef](#)]